THERMAL STRESS ANALYSIS OF SIMILAR AND DISSIMILAR WELDED JOINTS

Balram Yelamsetti[1], Rajyalakshmi G[2]

Thermal stresses can produce a non-uniform plastic deformation in the welded joints. An experimental investigation has been made to analyze the thermal stresses and thermal fields developed in the GTAW process for similar and dissimilar welded joints of Monel 400 and SS 316 using ERNiCrMo-3 filler wire. During welding, the temperature profiles of weldments have been measured using Infrared Thermography. The residual stress has been measured using X-Ray diffraction method. This paper reports on the weldability, microstructure studies and mechanical properties. The nature of Residual stresses has been observed in these welded joints and compared.

Keywords: IR Thermography, Residual Stresses, Similar Welds, Dissimilar Welds, Ni-based Filler Wire.

1. Introduction

Monel 400, a Ni-Cu based alloy, exhibits excellent fatigue strength and good ductility along with high corrosion resistance at elevated temperature. The Weldability of a nickel-based alloy is generally good, but some factors like metallurgical structure, residual stress & thermal distortion affect the service of the weld structure. Similarly, stainless steels are iron-based alloys, having good ductility, toughness and excellent resistance at high temperatures, and they are often referred as heat-resisting alloys [1]. Gas Tungsten Arc Welding (GTAW) process is extensively used for joining of metals and alloys in most of the aircraft industries, chemical and nuclear plant fabricators, rocket and missile fabricators [2]. Most often, Ni-based alloys along with other base metals like stainless steels are welded. Usually, they take advantage of the unique characteristics of weld metal which would allow it to provide better properties than that of base metal. These types of applications are most often found in nuclear, petrochemical and marine applications where the welds are usually exposed to higher temperatures [3-5]. The above base materials make it suitable for the applications mentioned, because of their weld properties and hence, deserve mention in joining the similar and dissimilar base materials. Selection of a proper filler material is necessary so that, it suits both the base materials when a dissimilar joint has to be made [6]. The Ni-base alloy filler metals convey excellent resistance towards oxidizing and reducing environments

[1] School of Mechanical Engineering, Vellore Institute of Technology, Vellore, India
[2] Associate Professor, School of Mechanical Engineering, Vellore Institute of Technology, Vellore, India, e-mail: rajyalakshmimed@gmail.com

just like any other Ni-based base material [7]. Though references are limited regarding the usage of the filler materials that would suit the discussed material combinations, a choice of ERNiCrMo-3 has been made based on its composition, i.e., it consists of Ni as a major proportion of the filler material along with other alloying elements like Cr and Mo. Welds that are made out of dissimilar material combinations are usually prone to residual stresses and thermal distortions which are caused due to differences in the thermal properties. Hence, to refine the weld parameters to form a welded joint, it requires first to analyze the occurrences of failures because of the dissimilarities in the thermal properties.

The inherent local non-uniform heating and cooling cycle associated with fusion-welding process results in thermal stresses and strains. These induced stresses can reduce the service life of a welded structure [8]. The weld-induced residual stresses and distortions are unfavorable as they can cause serious problems, such as hydrogen-induced cracking and stress corrosion cracking. These stresses are generally said to be thermally induced stresses, which can be permanent. As a result, the structure develops distortion [9]. As the Coefficient of Thermal Expansion (CTE) for Monel 400 and SS316 are close, it does not cause the thermal distortions [3, 10]. Further, these induced thermal stresses in joint influence the mechanical behavior of the weld material when external stresses are applied [11]. So, it is essential to understand the formation of residual stress and the effects of the failure of the welds of similar and dissimilar Monel 400 and SS 316. The nature of these thermally induced stresses can be either tensile or compressive which can influence the weld by increasing or decreasing the overall strength of the weld joint. For example, compressive stresses near to the weld zone can increase the yield strength of the welded joints [12]. Residual stresses in weldments are measured both by destructive and non-destructive methods. The X-ray diffraction technique, one of the Non Destructive Techniques (NDT), has been considered most suitable [13] and is used for the measurement of residual stresses in this investigation. The multi-pass TIG welded joints exhibited higher residual stresses and distortions, because of multiple heating and cooling cycles [13]. The higher heat input will cause more residual stresses near the weld zone, which can be minimized with a Heat Sink Welding (HSW) process. This HSW process can change the state of residual stresses from tensile to compressive after welding [14]. The magnitude and distribution of residual stresses are also influenced by the type of weld joint and thickness of materials. Smaller residual stresses were observed in the case of thick plates, since the thickness of the plates have been dominating causing a low thermal cycle in a particular region [15].

Residual stresses along with the Heat Affected Zone (HAZ) width, bead geometry are affected by thermal cycles, and hence, this study concentrates on the determination of precise temperature distribution characteristics and thermal field profiles which form the prerequisite. Since, Infra-Red (IR) thermography being one

of the promising NDE technologies to analyze the induced isotherms in welding [16], it is used to plot the temperature profiles during the welding process. It is well known as in situ temperature profile data logger, which measures the surface temperature by measuring the wavelengths of emitted infrared energy from the object [17]. The temperature profiles captured using IR thermography tool to validate the simulation results developed by the thermal cycles using finite element analysis is an indication that the profiles given by IR thermography are close and accurate enough to study the temperature gradients [18]. The temperature measurements from the data logger and their validations have been carried out for experimental analysis [19].

From the open literature review, it has been found that not much work has been done on residual stress analysis in the similar and dissimilar welded joints of Monel 400 and SS 316. Also, very few results have been reported in the studies using Infrared Thermography to measure the temperature during fusion welding process. In the present study, the GTAW process has been employed to join the similar and dissimilar metals of Monel 400 and SS 316. The filler wire ERNiCrMo-3 is used for a variety of welded joints to produce high strength welded structure which as resistance to corrosion environments. An experimental analysis of thermal cycles and residual stresses has been made on the welded joints. The microstructures and mechanical properties of similar and dissimilar welds while using ERNiCrMo-3 as filler in all the specimens have been studied to find the causes for the residual stresses and failure of the weld joints.

2. Experimental details

The base metals, Monel 400 and SS 316 plates of (0.15 x 0.08 x 0.005) m dimension have been considered for single V groove-butt welding using constant current GTA welding. The groove configuration of weld joint is clearly shown in Fig. 1. The ERNiCrMo-3 having diameter of 2.4 mm has been employed as the filler metal. Tables 1 and 2 give information on the chemical composition and mechanical properties [1, 3] of base and filler wire. The physical properties of base materials are given in Table 3. During welding, Argon shielding gas with a flow rate of 15 lpm has been used to prevent the oxidation of the weld and base metals. The welding processes have been carried out with three different combinations of base metals. The process parameters, heat input and welding speed listed in Table 4 are considered for welding of base metals. The arc efficiency of GTA welding process (η) has to be considered as 70% [20]. The welding speed and heat input have been calculated using Eq. 1 and 2. These weldments are developed using LINCOLN 375 manual welding machine as shown in Fig. 2 (a) and corresponding welded joints are obtained as shown in Fig. 2 (b). After the welding process, the weldments have been inspected for internal defects. From the confirmation of X-

ray radiographic test, the residual stresses have been measured using X-ray diffraction method. Further, the weldments had cut into different welding coupons to study the microstructures, micro hardness and tensile properties according to ASTM standards. The area selected for the above mentioned test as shown in Fig. 3.

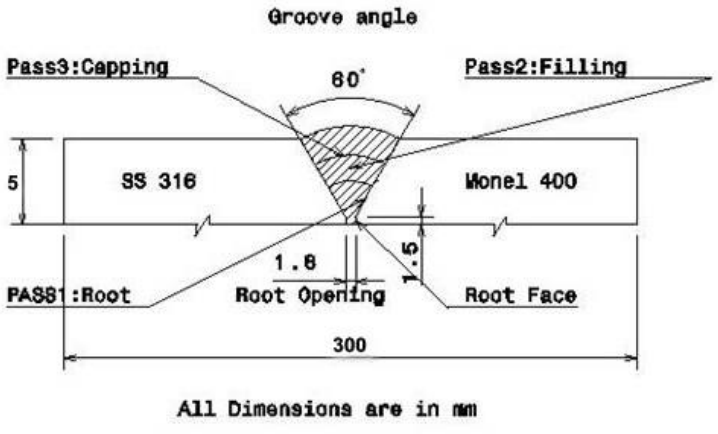

Fig. 1. Schematic diagram of weld groove design

Table 1

Chemical composition of Filler and Base metals

Filler metal/ base	Ni	Fe	Cu	Cr	Mn	C	Mo	Si	Others
ERNiCrMo-3	Rem	5.0	0.5	21.5	0.5	0.1	9.0	0.5	Co-9.0, Nb-3, Ti-0.4
Monel 400	Rem	2.5	31.5	---	1.6	0.12	---	0.4	----
SS 316	10.4	Rem	---	17.9	2.0	0.08	2.1	0.4	P- 0.002

Table 2

Mechanical properties of Filler/Base metal

Filler/Base metal	Ultimate Tensile Strength (MPa)	0.2% Yield Strength (MPa)	% of Elongation	Hardness	
				HRB	HV
ERNiCrMo-3	760	450	35	95	214
Monel 400	483	215	30	70	160
SS 316	520	241	40	80	198
Where, HRB-Rockwell Hardness Number, HV-Vicker's Microhardness Value					

Table 3

Physical properties of base metals

Base metal	Density (kg/m^3)	Elastic modulus (MPa)	Coefficient of thermal expansion $x10^{-6}$ (m/m/ K)		Thermal conductivity (W/m K)
			At 294 K	At 1373 K	
Monel 400	8380	$179x10^3$	13.9	18.5	21.8
SS 316	7870	$190x10^3$	15.2	19.6	13

Table 4

Parameters used during the welding process

Cases	Pass No	Current, I (A)	Voltage, V (V)	Heat input, Q (W)	Welding time (s)	Welding speed (mm/s)
S_1	Pass-1	120	14.5	1218.00	44.5	1.80
	Pass-2	130	14.5	1319.50	38	2.11
	Pass-3	130	14.5	1319.50	52	1.54
S_2	Pass-1	125	14.5	1268.75	54	1.48
	Pass-2	130	14.5	1319.50	36.5	2.19
	Pass-3	130	14.5	1319.50	48	1.67
S_3	Pass-1	130	14.5	1319.50	55	1.45
	Pass-2	135	14.5	1370.25	36.4	2.20
	Pass-3	135	14.5	1370.25	46	1.74

$$\text{Efficiency of heat source } (\eta) = \frac{Energy\ transferred\ to\ the\ workpiece\ (Q)}{Energy\ generated\ by\ the\ heat\ source}$$

$$\text{Heat input } (Q) = \eta * VI \tag{1}$$

$$\text{The welding speed} = \frac{Welding\ length}{Welding\ time} \tag{2}$$

Fig. 2. (a) LINCON 375 manual welding machine, (b) Welded joints image (S_1, S_2 and S_3)

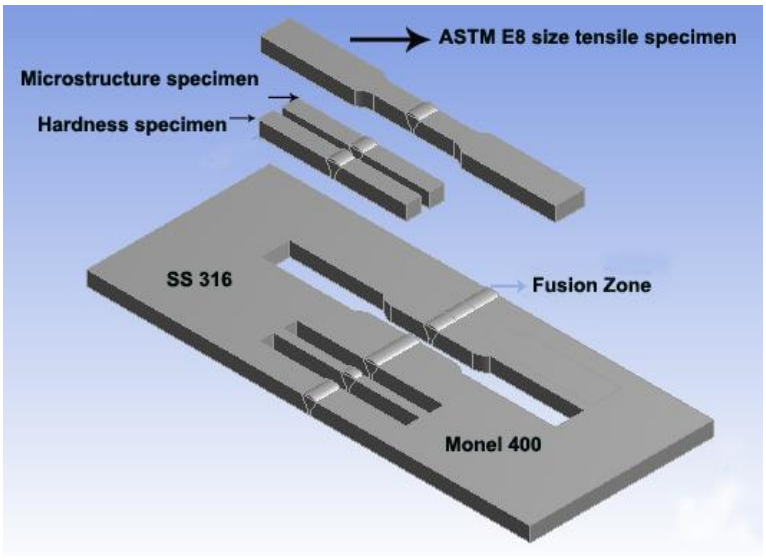

Fig. 3. Schematic representation of butt joint and various test specimens

2.1 Infrared Thermography

The Forward-Looking Infra-Red (FLIR) Tool plus has been used to analyze data obtained from the data logger within the visual zone to study temperature fields on three samples at all locations along the welding direction. IR thermography is well known for in situ temperature profiles which have the capability of measuring temperature in the range of 253 K to 2273 K. This infrared camera is attached to the logger which allows for in situ visualization and also stores information regarding temperature distribution over the entire surface of the specimens under the visual zone. The initial temperature of base metals is 303 K. In order to start the function of IR data logger the emissivity values of the material under inspection have to be entered, before starting the welding process. From the scientific data available in the literature on materials, the emissivity of the SS 316 and Monel 400 has been taken as $\varepsilon = 0.72$, $\varepsilon = 0.54$ respectively. A snapshot of the visual data zone of three cases has been shown in the Fig. 4.

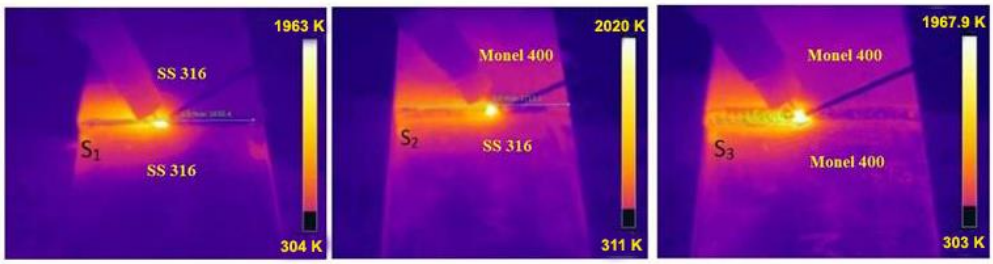

Fig.4. IR Thermography images (S_1, S_2 and S_3) cases

2.2 Residual stress measurement – XRD Technique

X-rays are employed for measuring stress in the crystalline materials. It involves X-Ray Diffraction (XRD) measurement of changes in interplanar spacing of a stressed metal which may lead to the formation of residual stresses. Diffraction technique has been carried out for measuring stresses in the similar and dissimilar welded joints. The angle of reflection is used to determine the change in the interplanar spacing compared to the stress free state. This in turn is used to determine the sum of the principle stresses at the surface of the welded joint with the help of Bragg equation as given below.

$$n\lambda = 2d \sin\theta \qquad (3)$$

Where λ is the order of reflection and d is the interplanar lattice spacing. The value of interplanar spacing, d, is used in the elastic stress-strain relationship to determine the stresses in welded joints. Diffraction technique measures only the surface strains and therefore, the residual stress $\sigma_{\emptyset}$ can be determined using the following equation [10].

$$\sigma_{\emptyset} = \frac{m}{d_0}\left(\frac{E}{1+v}\right) \qquad (4)$$

Where v=poisson's ratio, d_0=interplanar unstressed lattice space and E=elastic modulus. The $sin^2\psi$ method is used for calculating the residual stresses in welded plates. Vanadium filtered Mn-Kα radiation of wavelength λ=1.0744291(°A) was diffracted from the (311) planes in (for S_2 at the weld zone) at $2\theta = 156.32^0$. For the similar joints of S_1 and S_3, the residual stresses have been measured at one side of the plate from the weld center line. The induced stresses are calculated using Eq. 4 given above, by taking the slope (m) from lattice space d against $\sin^2\psi$. This value has been found to be -212.76 MPa at weld zone, which is taken as the measure of residual stress.

2.3 X-Ray Radiography

In this study, CEREM 235 Radiography machine has been used for inspecting internal defects in weldments of similar and dissimilar metals, Monel 400 and SS 316. The weldments have been characterized for determining any macro/microscopic defects using X-ray radiography technique according to ASME SEC-VIII standard. X-rays are produced when high speed electrons, in the form of a beam called cathode ray, strike a metal target placed in an x-ray tube. The velocity at which the electrons strike the target is determined by the tube voltage, where the tube voltage is the potential difference between the sources of electrons. The X-ray source is used to examine the welded joints of short wavelength and with an

exposure time of 120 s. The source voltage of 150 keV and a current of 3.5 mA have to be maintained.

3. RESULTS AND DISCUSSIONS

3.1 Macro and Microstructure Studies

From the radiography NDT analysis shown in Fig. 5, the observation has been made clearly and has been confirmed that there is no evidence of internal defects. On inspecting the macro structures of welded joints obtained for three samples, namely S_1, S_2, and S_3 by using metallurgical microscope, images of the weld bead configuration as shown in Fig. 6 (a), 7 (a) and 8 (a) revealed that there is no formation of macro porosity in any of the specimens. The metallurgical studies made on three samples have clearly shown that there is a growth of dendritic structure which is caused because of effective diffusion of alloying elements and base materials as shown in Fig 6. In the case of S_1, the HAZ of SS has shown a twinned and coarse grain structure having a grain size of G=6 whereas, base material grain size is reported as 7 with a twinned grain structure. The HAZ micro photographs have shown the formation of secondary phases at the interface zone of SS 316 with lengths less than 50 μm. In the case of S_2, the secondary phase formation has been observed at the interface of SS 316 only, because of alloying elements present in the filler composition. It is also confirmed that from thermography results SS316 of HAZ on exposure to high temperature of about 1320 K led to the formation of secondary phases (sigma phases, chi phases). The austenitic grain structure has been observed in HAZ of Monel 400 and there is no change is hardness value in the base and HAZ of Monel 400. In the case of S_3, the HAZ of Monel 400 has shown the austenitic grain structure similar to that of Monel 400 base metal side of S_2. It is also evident from the tensile test that, the failure of welded joints has occurred in the base material because there is proper dilution of filler material with base materials of SS 316 and Monel 400. This type of failure is observed in all the three cases as shown in Fig. 10.

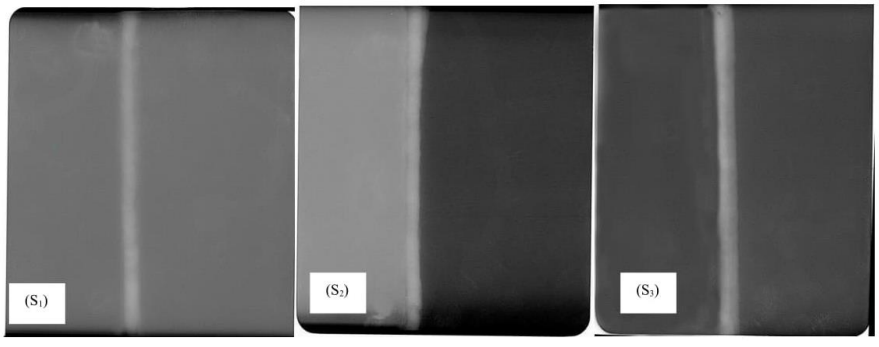

Fig. 5. Radiographs of S_1, S_2 and S_3 cases

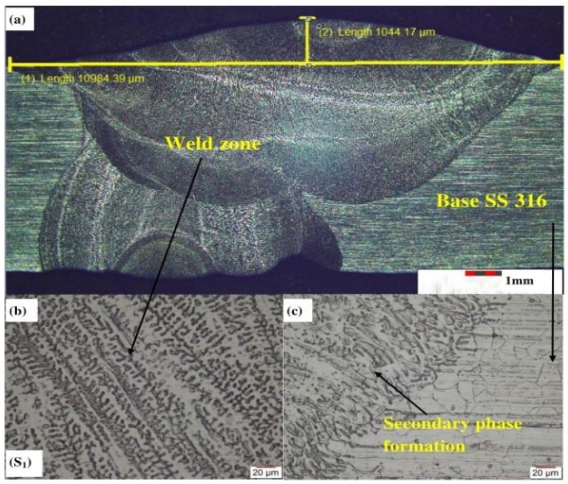

Fig. 6. Microstructure of similar welded joint (S_1)

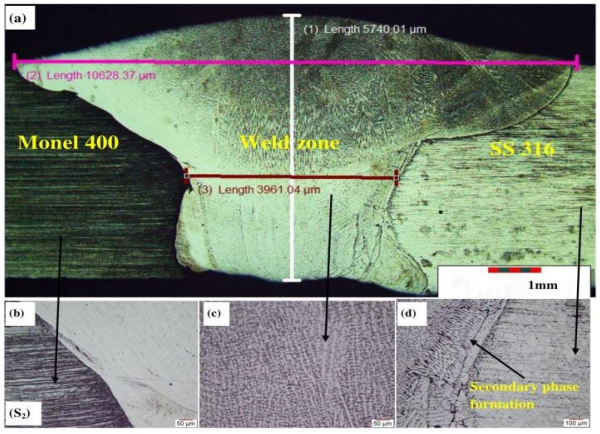

Fig. 7. Microstructure of dissimilar welded joint (S_2)

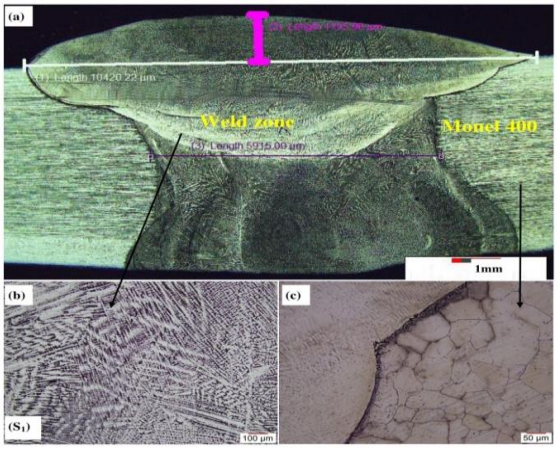

Fig. 8. Microstructure of similar welded joint (S_3)

3.2 Micro hardness studies

The series of hardness values obtained from the Vickers micro hardness test are plotted across the weld zone and HAZ. Hardness values have been measured at 0.2 mm indentation between each. Hardness profiles are shown in Fig. 9, on the welded joints of similar and dissimilar SS 316 and Monel 400 with filler metal ERNiCrMo-3. From the hardness profiles, it is clearly shown that the average hardness value of 212.6 HV has been observed at the weld zone in all the three cases (S_1, S_2, and S_3). The observation of microstructure reveals dendritic structure at the weld zone in all the three cases. Hence, there is an increase in hardness value compared to the base and HAZ of welded joints. On the other hand, the average hardness value of base metal, Monel 400, has been found to be 159.5 HV and 200.3 HV for SS 316 side. There is no change in hardness value in HAZ of Monel 400 and base material. It has also been observed and also seen that there are no structural changes in microstructure, but a small variation in hardness has been observed on HAZ of SS 316.

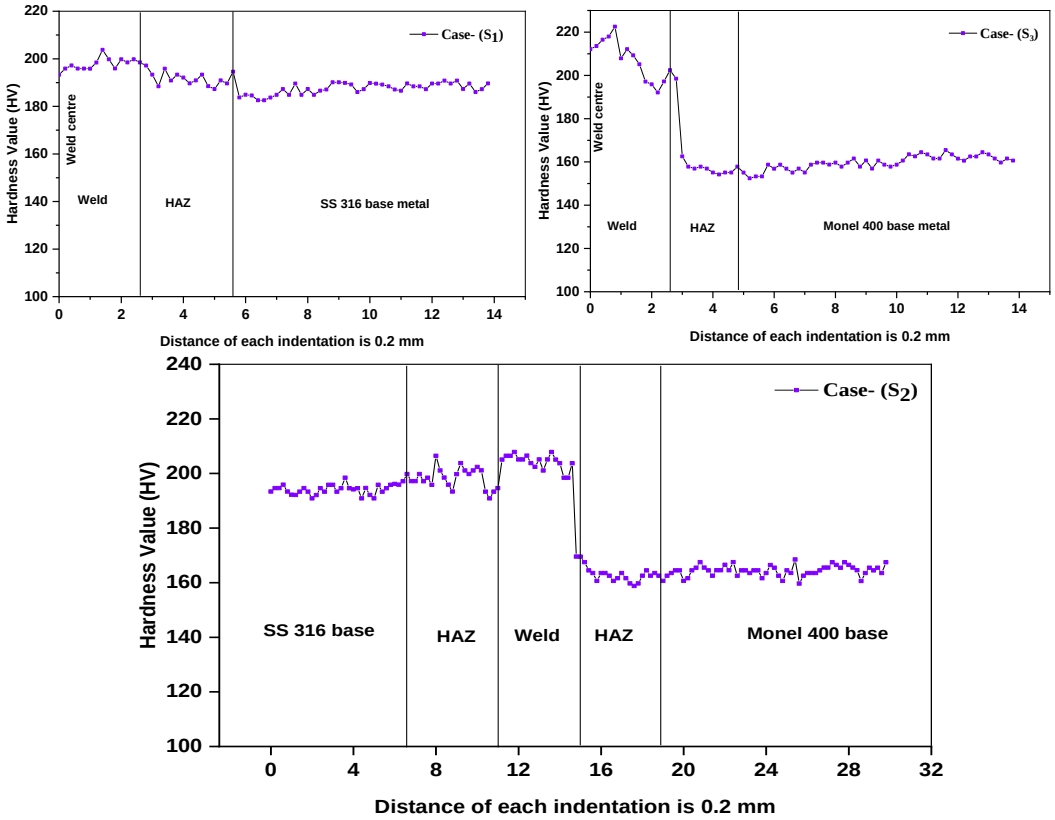

Fig. 9. Variations of micro hardness for S_1, S_2 and S_3 cases

3.3 Tensile studies:

In this experiment, the tensile test has been carried out as per the ASTM E8 procedure to study the behavior of welded joints when exposed to tension. The test results are shown in Table 5. In the aforementioned three specimens, the failures occurred after the HAZ and plastic deformation occurred at the fracture site (approx 30 -50% reduction in area) indicating a ductile failure as shown in Fig. 10. In the case of S_1, the fracture is observed away from the HAZ, indicating the weld strength to be greater than that of the base material in spite of small secondary phase zone formation in the weld zone owing to the proper dilution between base material and filler wire. In the case of S_2, a small segregation of secondary phase about the size of 50 microns has been observed. In the case of S_3, the failure has been predicted as Monel is weaker, hence, owing to a stronger weld joint.

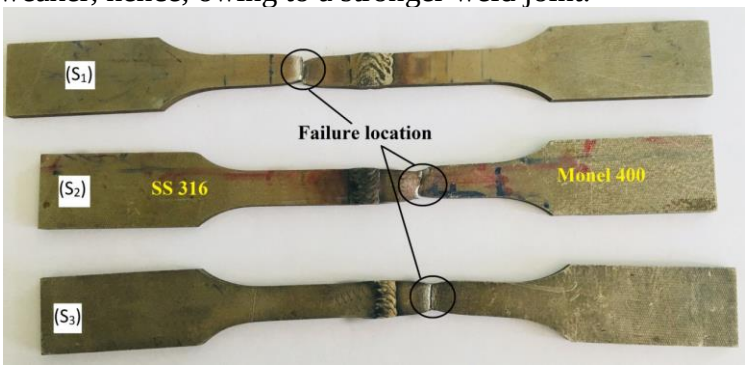

Fig. 10. Specimens fractured under tensile test (S_1, S_2, and S_3)

Table 5

Tensile properties of welded joints

Cases	UTS (MPa)	YS (MPa)	% of Elongation	Failure location
S_1	556.94	261.13	53.58	Base metal SS316
S_2	543.67	252.73	42.13	Base metal Monel 400
S_3	533.82	243.18	36.74	Base Monel 400

3.4 Temperature field

From the IR thermography, the temperature distribution has been analyzed and temperature profiles have been plotted for three samples as shown in Fig. 11, 12, and 13. The temperature gradients have been observed in the transverse direction in all the cases. The temperature profiles are also plotted in weld direction as shown in Fig. 13 for both base materials of Monel 400 and SS 316 HAZ in case of S_2.

In case of S_1, an increment in temperature profile has been observed in each progressive pass. In the root pass welding, the maximum temperature of 1767 K has been recorded. Later in the 3rd pass, the maximum temperature of 2025 K has been recorded as a result of high HAZ. In case of S_2, there is a significant

temperature difference which has been recorded in HAZ of Monel 400 as compared to the HAZ of SS 316 indicating the difference in the thermal properties as shown in Fig. 14. Although a continuous heat input has been given to the weldments, the maximum temperature that has been recorded in the third pass is 1970 K which is closer to the temperatures recorded in S_1. In S_3, as Monel 400 has good thermal conductivity, and it dissipates heat at a faster rate compared to S_1, smaller HAZ has been observed and shown in Fig. 15. Temperature values have been measured in the three cases at weld center and 15 mm away from the weld line in both sides of similar and dissimilar welded joints have been given in Table 6. During the course of welding, it is found that there is an increase in number of improper temperature gradients when continued with more passes.

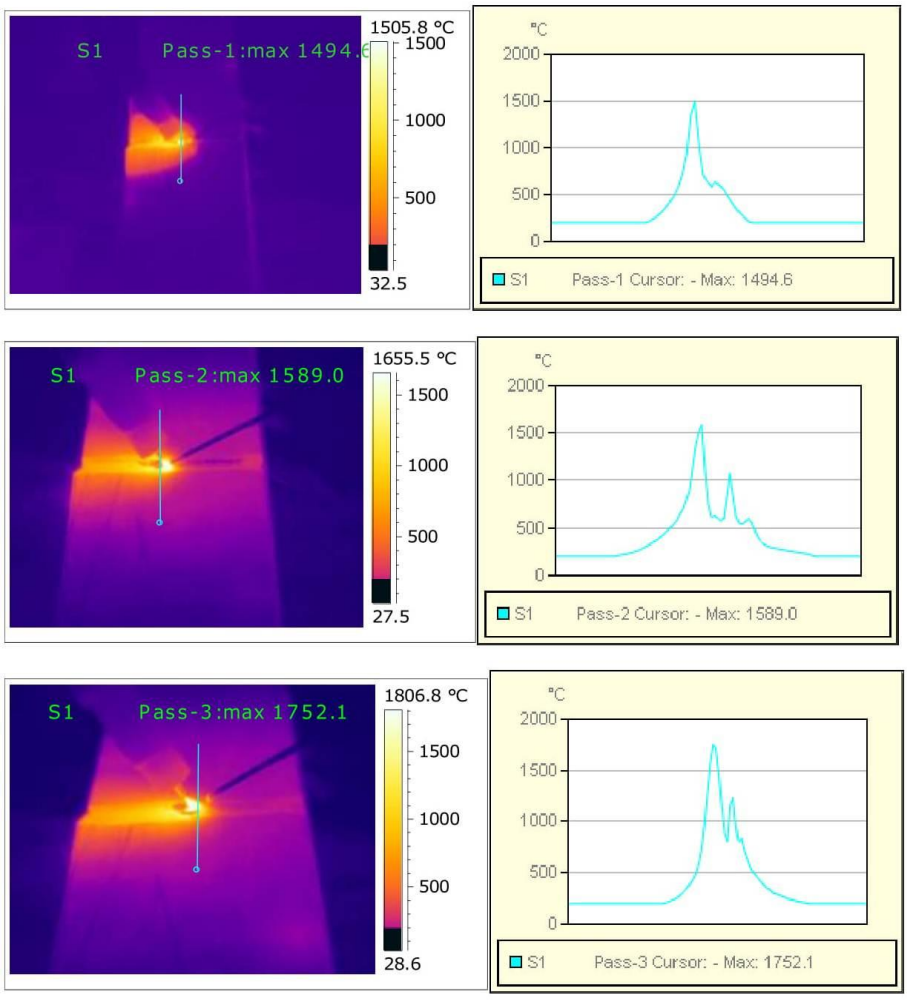

Fig. 11. Infrared temperature profiles in S_1 case

Table 6

Temperature measurement in three cases

Cases	Location of point	Temperature (K)		
		Pass-1	Pass-2	Pass-3
S_1	15 mm away from weld line	1138	1237.4	1297.8
	Weld center	1767.6	1862	2025
S_2	15 mm away from weld line of Monel	1107.34	1197.2	1262.4
	Weld center	1708.8	1887.7	1970
	15 mm away from weld line of SS	1128.4	1249.4	1320.45
S_3	15 mm away from weld line	1116	1185.6	1265.5
	Weld center	1772.6	1781.8	1957.3

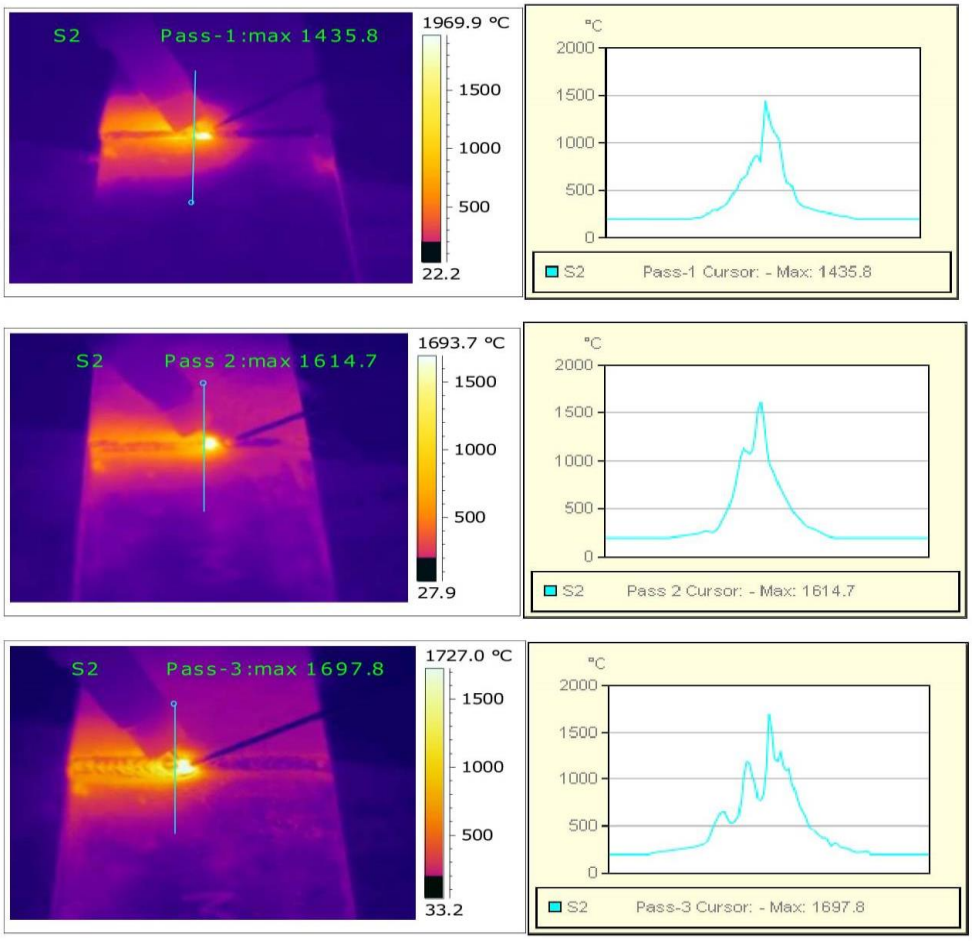

Fig. 12. Infrared temperature profiles in S_2 case

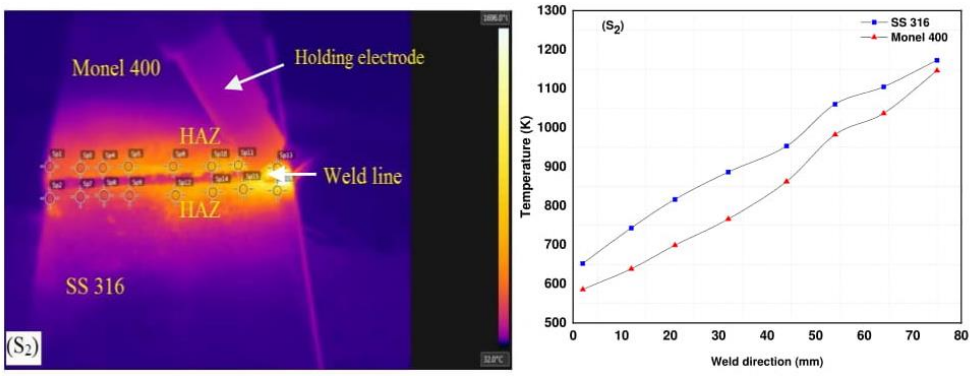

Fig. 14. Temperature measurement in HAZ (S_2)

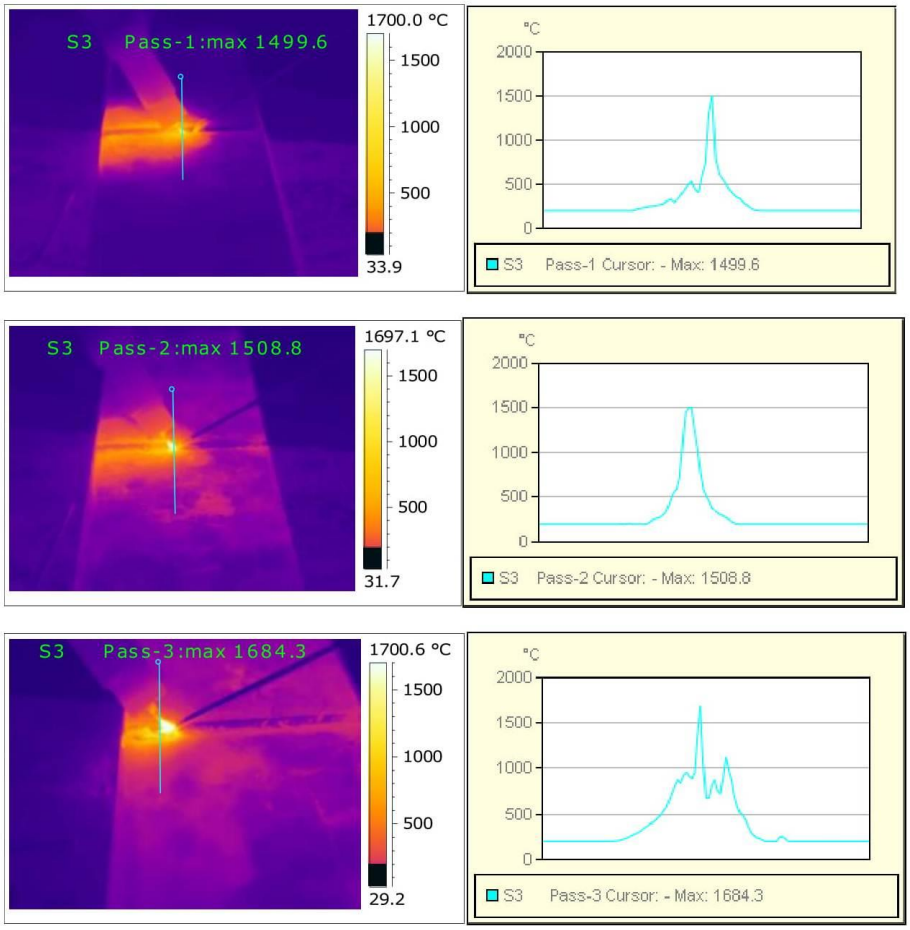

Fig. 13. Infrared temperature profiles in S_3 case

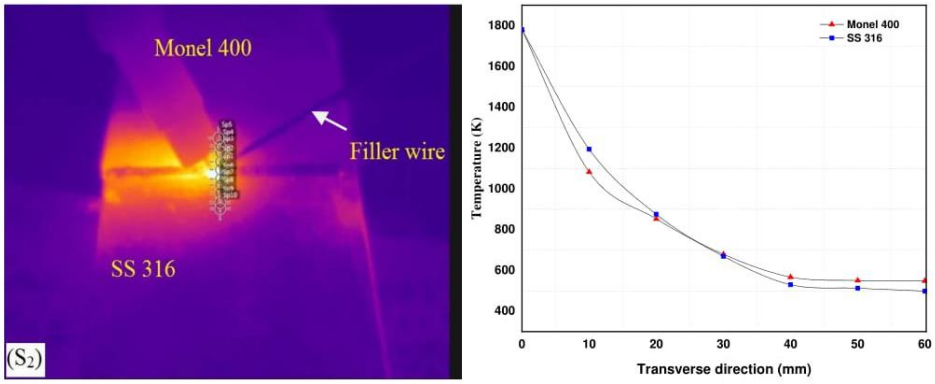

Fig. 15. Temperature profiles in the transverse direction (S_2)

3.5 Characterization of residual stress

Fig. 16 shows the residual stress distribution in the transverse direction (perpendicular to the fusion zone) for three cases. Uneven temperature gradients are the main cause for the development of the residual stresses in the welded joint. XRD test has confirmed the results of the variation of the stress zones on and about the weld joint which are indicated in the Fig. 16. S_1 has a compressive stress (37.85 MPa) in the HAZ and complete tensile (57.38 MPa) in the weld zone. With a thermal conductivity less on SS side, heat transfer is low, slow cooling occurs resulting in the tensile stress in the weld zone and compressive stress in the HAZ. S_3 has shown compressive stress (167.54 MPa) in weld zone and tensile (35.12 MPa) in the HAZ. S_2 has shown the formation of compressive stresses in weld zone and tensile in the HAZ on Monel 400 side similar to that of S_3 HAZ and compressive in the HAZ on SS 316 side similar to S_1 HAZ. Because of high thermal conductivity of the base material, the weld tries to compress due to fast cooling resulting in high compressive stresses in the weld zone. Upon comparison of the HAZ of S_1 and S_2, it is also observed that the magnitudes of the compressive stress in the HAZ on SS side have increased in S_2. A similar comparison is made between S_2 and S_3 wherein the tensile stresses in the HAZ on Monel has increased in S_2. As a whole, there is an overall possibility of the formation of compressive stresses in the weld and HAZ of S_2. This can be the major cause for the failure of the weld metal and can only be avoided by creating suitable weld temperature gradients with proper heat input rates so as to give sufficient time to form uniform phases throughout the weld zone.

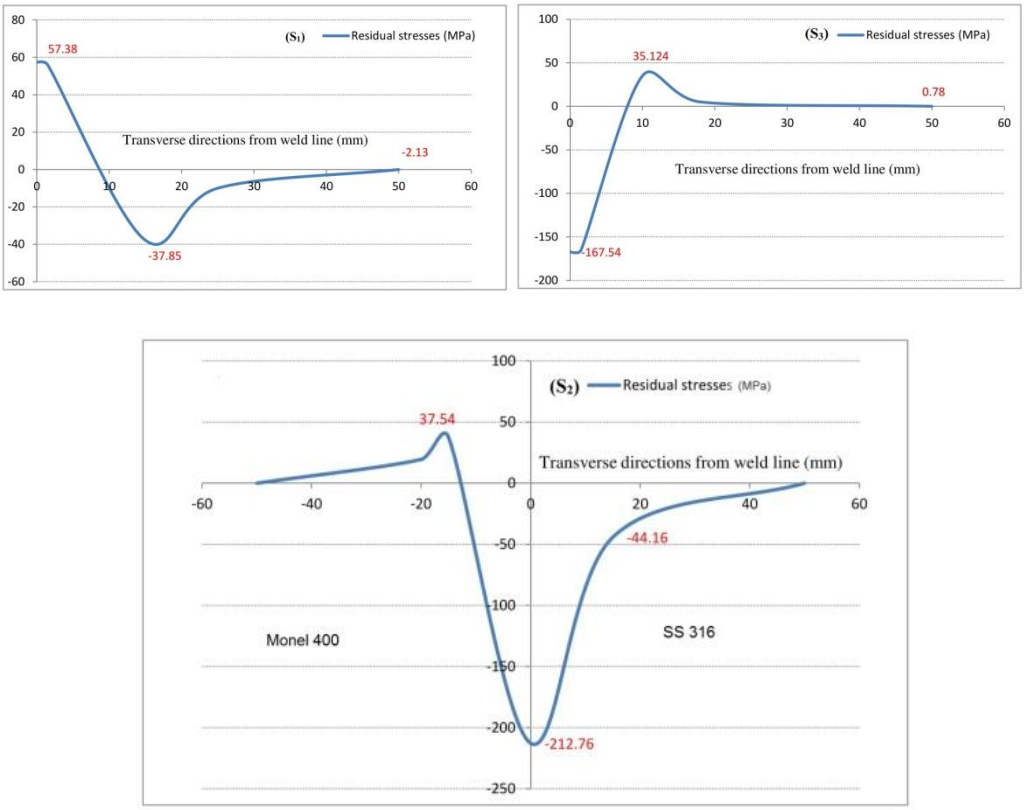

Fig. 16. Residual stress distribution for three samples S_1, S_2, and S_3

4. Conclusions

In this experimental analysis, temperature fields, residual stress distribution, microstructures and mechanical properties of similar and dissimilar Monel 400 and SS 316 welded joints have been reported.

- GTAW process has been performed successfully on defect free welds of similar and dissimilar materials, namely, Monel 400 and SS 316 by using ERNiCrMo-3 filler wire.
- Similar and uniform austenitic structure has been observed in all the weld zone of three cases, hence, Monel 400 and SS 316 weldments gives the approximately equal mechanical properties.
- It is observed that in tensile testing of all three samples of S_1, S_2, and S_3, the failure has occurred in the base metal, hence, ERNiCrMo-3 is found to be suitable for joining of similar and dissimilar Monel 400 and SS316, compressive stresses in fusion and HAZ are protecting.

- The weldment of S_2 has demonstrated the ultimate tensile strength (543 MPa), yield strength (252 MPa) and % of elongation (41.56) which are very close to the similar joints of S_1 and S_3. Even mechanical properties are having close values in both dissimilar materials.
- Variations of thermal gradients have led to the formation of secondary phases at the interface of SS316 base metal, but these phases did not contribute to the failure of the welds under tensile test.
- IR Thermography had been found to be a potential tool for measuring temperature, during GTA welding process, measurements were found in the fusion zone of weldments. Further, it can be used for control of weld bead geometry during GTA welding.
- The transverse residual stresses in the welded joints are within the yield strength limit of base materials only.
- Due to variations in thermal gradients, the transverse residual stresses have been developed in the weld and HAZ of welded joints. This can be minimized by controlling of temperature gradients in the weld area with proper heat input rates.

R E F E R E N C E S

[1] *John C. Lippold and Damian J. Kotecki*, Welding Metallurgy and Weldability of Stainless Steels,Wiley, Interscience, 2005.

[2] *R. S. Parmer*, Welding Engineering and Technology, second edition, Khanna Publishers, 2016.

[3] *J. R. Davis*, ASM Specialty Handbook, Nickel, Cobalt, and Their Alloys, 2000.

[4] *K. Devendranath Ramkumar, S. V. Naren, V. R. Karthik Paga, A. Tiwari, and N. Arivazhagan*, Development of pulsed current gas tungsten arc welding technique for dissimilar joints of marine grade alloys, J. Manuf. Process., **vol. 21**, pp. 201–213, 2016.

[5] *D. Mishra, M.K. Vignesh , B. Ganesh Raj, Pruthvi Srungavarapu, K. Devendranath Ramkumar, N. Arivazhagan, S. Narayanan*, Mechanical characterization of Monel 400 and 316 stainless steel weldments, Procedia Eng., **vol. 75**, pp. 24–28, 2014.

[6] *K. D. Ramkumar, A. Chandrasekhar, A. K. Singh, S. Ahuja, and N. Arivazhagan*, Effect of Filler Metals on the Structure–Property Relationships of Continuous and Pulsed Current GTA Welds of AISI 430 and AISI 904L, Metallogr. Microstruct. Anal., **vol. 4**, no. 6, pp. 525–541, 2015.

[7] *K. D. Ramkumar, N. Arivazhagan, and S. Narayanan*, Effect of filler materials on the performance of gas tungsten arc welded AISI 304 and Monel 400, J. Mater., **vol. 40**, pp. 70–79, 2012.

[8] *Dong*, Residual stresses and distortions in welded structures: a perspective for engineering applications, Sci. Technol. Weld. Join., **vol. 10**, no. 4, pp. 389–398, 2005.

[9] *P. J. Withers and H. K. D. H. Bhadeshia*, Residual stress. Part 1–measurement techniques, Mater. Sci. Technol., **vol. 17**, no. April, pp. 355–365, 2001

[10] P. *D. Desai and C. Y. Ho*, Thermal linear expansion of nine selected AISI stainless steels, 1978.

[11] *P. S. Prevey*, X-ray diffraction residual stress techniques, Met. Handbook. 10. Met. Park, no. 513, pp. 380–392, 1986.

[12] *B.I Ischner and N.J. Grant*, Materials research and engineering, 1987.
[13] *P. Vasantharaja, V. Maduarimuthu, M. Vasudevan, and P. Palanichamy*, Assessment of residual stresses and distortion in stainless steel weld joints, Mater. Manuf. Process., **vol. 27**, no. 12, pp. 1376–1381, 2012.
[14] *Y. S. Yegaie, A. Kermanpur, and M. Shamanian*, Numerical simulation and experimental investigation of temperature and residual stresses in GTAW with a heat sink process of Monel 400 plates, J. Mater. Process. Technol., **vol. 210**, no. 13, pp. 1690–1701, 2010.
[15] *J. Xia and H. Jin*, Numerical study of welding simulation and residual stress on butt welding of dissimilar thickness of austenitic stainless steel, Int. J. Adv. Manuf. Technol., **vol. 91**, no. 1–4, pp. 227–235, 2017.
[16] *M. Vasudevan, M. N. Chandrasekhar, M. V Maduraimuthu, A. K. Bhaduri, and B. Raj*, Real-time monitoring of weld pool during GTAW using infra-red thermography and analysis of infra-red thermal images, Weld. World, **vol. 55**, no. 7–8, pp. 83–89, 2011.
[17] *C. Meola and G. M. Carlomagno*, Recent advances in the use of infrared thermography, Meas. Sci. Technol., **vol. 15**, no. 9, 2004.
[18] *K. C. Ganesh, M. Vasudevan, K.R. Balasubramanian, N. Chandrasekhar, S. Mahadevan, P. Vasantharaja and T. Jayakumar*, Modeling, prediction and validation of thermal cycles, residual stresses and distortion in type 316 LN stainless steel WELD joint made by TIG welding process, Procedia Eng., **vol. 86**, pp. 767–774, 2014.
[19] *R. Komanduri and Z. . Hou*, A review of the experimental techniques for the measurement of heat and temperatures generated in some manufacturing processes and tribology, Tribol. Int., **vol. 34**, no. 10, pp. 653–682, 2001.
[20] *S. A. A. Akbari Mousavi and R. Miresmaeili*, Experimental and numerical analyses of residual stress distributions in TIG welding process for 304L stainless steel, J. Mater. Process. Technol., **vol. 208**, no. 1–3, pp. 383–394, 2008.